

Nanowire Templated Semihollow Bicontinuous Graphene Scrolls: Designed Construction, Mechanism, and Enhanced Energy Storage Performance

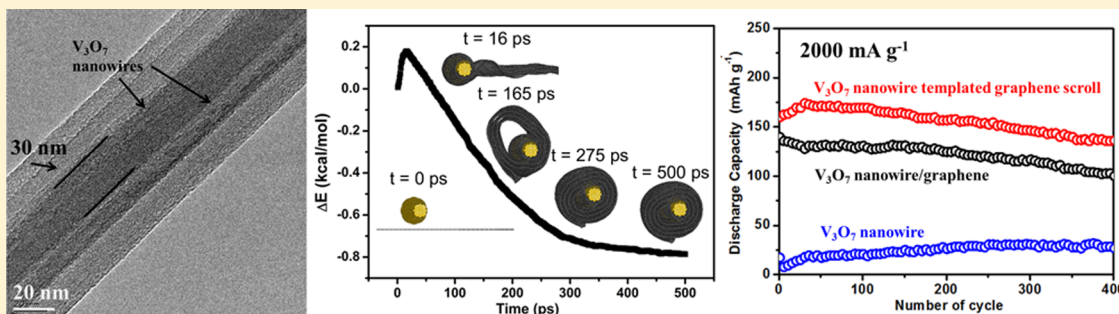
Mengyu Yan,^{†,||} Fengchao Wang,^{‡,||} Chunhua Han,^{*,†} Xinyu Ma,[†] Xu Xu,[†] Qinyou An,[†] Lin Xu,^{†,§} Chaojiang Niu,[†] Yunlong Zhao,[†] Xiaocong Tian,[†] Ping Hu,[†] Hengan Wu,^{*,‡} and Liqiang Mai^{*,†}

[†]State Key Laboratory of Advanced Technology for Materials Synthesis and Processing, WUT-Harvard Joint Nano Key Laboratory, Wuhan University of Technology, Wuhan 430070, People's Republic of China

[‡]CAS Key Laboratory of Mechanical Behavior and Design of Materials, Department of Modern Mechanics, University of Science and Technology of China, Hefei, Anhui 230027, People's Republic of China

[§]Department of Chemistry and Chemical Biology, Harvard University, Cambridge, Massachusetts 02138, United States

S Supporting Information



ABSTRACT: Graphene scrolls have been widely investigated for applications in electronics, sensors, energy storage, etc. However, graphene scrolls with tens of micrometers in length and with other materials in their cavities have not been obtained. Here nanowire templated semihollow bicontinuous graphene scroll architecture is designed and constructed through “oriented assembly” and “self-scroll” strategy. These obtained nanowire templated graphene scrolls can achieve over 30 μm in length with interior cavities between the nanowire and scroll. It is demonstrated through experiments and molecular dynamic simulations that the semihollow bicontinuous structure construction processes depend on the systemic energy, the curvature of nanowires, and the reaction time. Lithium batteries based on V₃O₇ nanowire templated graphene scrolls (VGSSs) exhibit an optimal performance with specific capacity of 321 mAh/g at 100 mA/g and 87.3% capacity retention after 400 cycles at 2000 mA/g. The VGSS also shows a high conductivity of 1056 S/m and high capacity of 162 mAh/g at a large density of 3000 mA/g with only 5 wt % graphene added which are 27 and 4.5 times as high as those of V₃O₇ nanowires, respectively. A supercapacitor made of MnO₂ nanowire templated graphene scrolls (MGSSs) also shows a high capacity of 317 F/g at 1A/g, which is over 1.5 times than that of MnO₂ nanowires without graphene scrolls. These excellent energy storage capacities and cycling performance are attributed to the unique structure of the nanowire templated graphene scroll, which provides continuous electron and ion transfer channels and space for free volume expansion of nanowires during cycling. This strategy and understanding can be used to synthesize other nanowire templated graphene scroll architectures, which can be extended to other fabrication processes and fields.

INTRODUCTION

Graphene, the first two-dimensional (2D) atomic crystal structure available to us, shows great mechanical stiffness,^{1,2} strength and elasticity,³ very high electrical^{4,5} and thermal conductivity,⁶ and large surface area.⁷ The outstanding properties of graphene have motivated intensive efforts to construct graphene-based materials, which have been widely used in energy storage^{8–10} and energy conversion^{11,12} devices, sensors,¹³ catalysis,^{14,15} and bioapplication.^{16,17} Most of the active materials are deposited on the surface of the graphene framework (2D, 3D) or encapsulated as a core in the graphene shell (0D). Nevertheless, graphene-based materials with well-

defined 1D and tens of micrometers in length have not been realized.

1D nanostructures are important in materials science and technology, since they have some unique properties associated with the bridge between micro- and nanoscale features¹⁸ and the confinement effect in the axial direction.^{19,20} Graphene scrolls (GSs) are 1D carbon materials normally formed through a graphene rolling mechanism which exhibits the theoretical possibility of encapsulating nanodroplets²¹ or other nanoma-

Received: August 31, 2013

Published: November 12, 2013

terials into the interior cavities^{22–24} due to the topology of the GSs. GSs provide open structures at both ends and interlayer galleries that can be easily intercalated and adjusted, which show great potential applications in energy storage.^{25–27} The most important is that GSs, formed by the roll-like wrapping of graphene sheets, enable wrapping nanowires/nanotubes in the scrolls in theory (Figure S1, Supporting Information). It was calculated that nanowires can activate and guide the self-assembly of planar graphene sheets on the nanowire/nanotube surface, which showed lower energy demands than the formation of pure GSs.^{28–30} However, such a self-assembly process has not yet been achieved in the experiments. In addition, the length of GSs, limited by the scale of graphene (less than 5 μm in traditional cases),³¹ is another challenge for the application of GSs in energy storage, sensors, and nanoelectronics.^{32–39} Longer GSs may provide novel opportunities for enhancing transport electrical and other physical properties through nanoscrolls over large length scales.

In this paper, V_3O_7 and MnO_2 are chosen as prototypes to demonstrate the “oriented assembly” and “self-scroll” construct mechanisms of nanowire templated graphene scrolls. There are two key dynamics processes in the self-assembly. The first is the rapid growth of nanowires and oriented assembly of the graphene sheets on the surface of the nanowire and then the self-scroll of graphene ribbons (Figure 1). Such a facile method

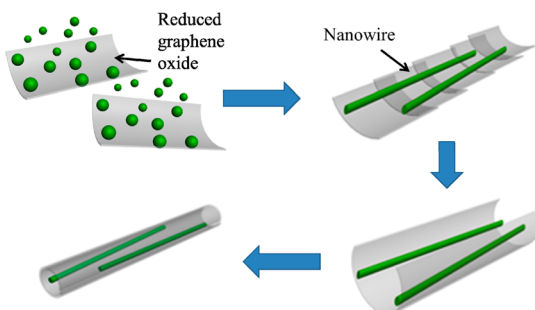


Figure 1. Construction processes of nanowire templated graphene scrolls. The green dots represent the precursor of the nanowire template and then formation into the nanowire. The gray sheets and scroll represent the reduced graphene oxide (rGO).

can break the length limitation of GSs determined by the size of graphene (GSs over 30 μm in length were achieved). Nanowires being rolled into the hollow cavities of GSs show a new synthesis strategy to introduce other materials into the cavities and greatly widen the application range of GSs or GS-based composite materials. Further experiments and molecular dynamics (MD) simulations results confirm the structure and construction mechanism of the V_3O_7 nanowire templated semihollow bicontinuous graphene scroll (VGS) architecture. The VGSs offer a unique combination of ultralong 1D graphene scrolls with semihollow structure and space confining effect for the nanowires without self-aggregation during cycling, thus allowing for a greater lithium ion storage capacity and stability. As a proof of concept, a cathode made of VGSs shows a high specific capacity of 321 mAh/g at 100 mA/g and leads to a great enhancement of cycling stability and rate capability with only 5 wt % graphene added. Furthermore, the oriented assembly and self-scroll strategy is also used in designing the construction of MnO_2 nanowire templated graphene scroll (MGSSs), which show morphology characteristics and enhanced energy storage performance similar to those of VGS. On the

basis of the same synthetic strategy, other matters can play the same roles as the template of the graphene scroll.

EXPERIMENTAL SECTION

Materials and Methods. The rGO was synthesized through a modified Hummer method.^{40,41} The hydrothermal method was used to synthesize the VGS with the as-prepared rGO suspension (~1 mg/mL). A 1.3 mmol portion of vanadium sol and aniline were mixed in a 100 mL beaker and stirred at room temperature for 30 min in a molar ratio of 1:0.03. Next, 13 mL of an rGO suspension (~5 wt %) was added to the mixture, which was then stirred at 25 °C for 1 h. The sample was then placed into a 100 mL autoclave and heated at 180 °C for 12–96 h. After washing and drying, a blackish green powder was obtained. The pure V_3O_7 nanowires (PV) were prepared through the same method above without addition of rGO. The V_3O_7 nanowire/graphene structure without nanowire templated graphene scrolls (VG) was prepared by mixing 13 mL of an rGO suspension with 1.3 mmol of PV and then drying at 80 °C for 24 h. The synthesis details of rGO, PV, and MGSS and fabrication details of electrochemical devices are further described in the Supporting Information.

Characterization. An X-ray diffraction (XRD) measurement was performed to investigate the crystallographic information using a D8 Advance X-ray diffractometer with a non-monochromated Cu $\text{K}\alpha$ X-ray source. Field-emission scanning electron microscopic (SEM) images and energy dispersive spectroscopic (EDS) line scans were collected with a JSM-7001F instrument at an acceleration voltage of 10 kV. Transmission electron microscopic (TEM) and high-resolution TEM images were recorded with a JEM-2100F STEM/EDS microscope.

MD Computational Details. All of the MD simulations in our present work were implemented in the large-scale atomic/molecular massively parallel simulator (LAMMPS).⁴² Simulations of the wrapping process of a nanowire by a monolayer graphene ribbon were carried out for 500 ps with a time step of 1.0 fs. The graphene ribbon was constructed with the length and width of 42.6 nm. The interactions among the carbon atoms in the graphene were described by the adaptive intermolecular reactive empirical bond order (AIREBO) potential.⁴³ The interactions between graphene and 1-nanometer-diameter nanowires were modeled by a Lennard-Jones (LJ) potential with a cutoff of 12 Å. LJ parameters were simply set to be $\epsilon = 5.0$ meV and $\sigma = 3.0$ Å, respectively. After the initial configuration was constructed, the model was equilibrated at $T = 450$ K with a Langevin thermostat for temperature control. During the run time, simulation snapshots were saved every 1.0 ps for postsimulation analysis.

RESULTS AND DISCUSSION

We choose V_3O_7 as the first prototype to demonstrate the construction, mechanism, and energy storage performance of nanowire templated semihollow bicontinuous graphene scrolls. The crystal structures have been characterized by XRD measurement. The obtained VGS and PV are both indexed to hydro V_3O_7 (028-1433) (Figure S2, Supporting Information). SEM and TEM observations were further employed to characterize the morphology and detailed structure of the products. It is important to note that the sizes of graphene sheets are only 1–2 μm . Notably, the low-magnification SEM image (Figure 2a) shows that the length of synthesized VGS is continuous over 30 μm , which is much longer than the scale of graphene. Focusing on the end of the V_3O_7 nanowire (Figure 2b) and GSs (Figure 2c), the V_3O_7 nanowires have been totally introduced into the cavity of the GSs. The length of V_3O_7 nanowires is 1–2 μm shorter than that of GSs, which equals the size of graphene. This phenomenon proves that the graphene sheets are assembled with the support of V_3O_7 nanowires. A TEM image of the synthesized nanowire (Figure 2d) demonstrates that the diameter of V_3O_7 nanowires is less

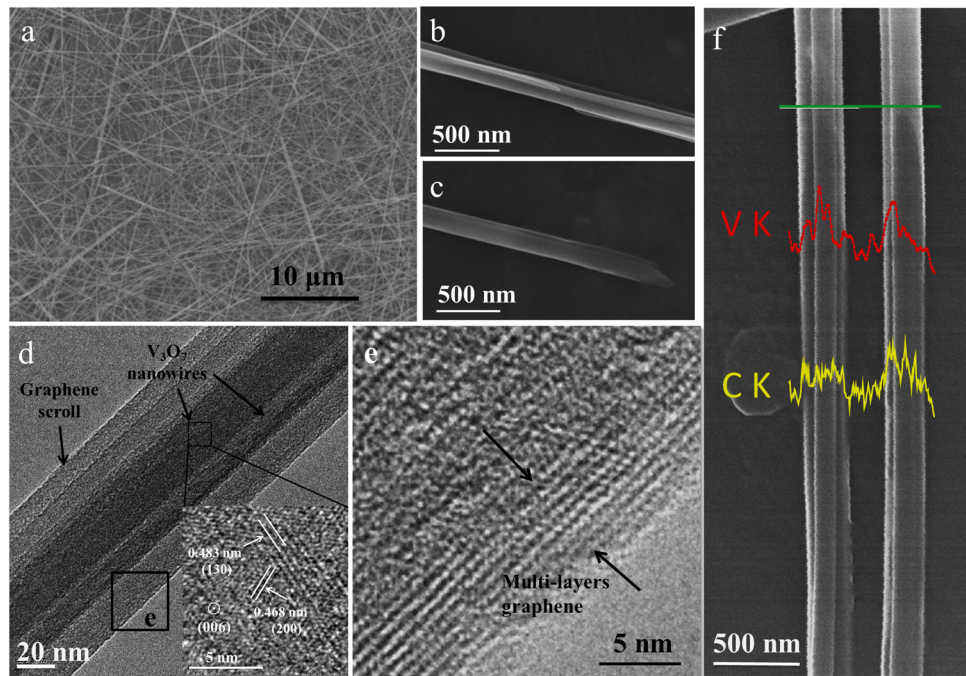


Figure 2. Structure of VGS: (a) SEM image of synthesized VGS at low magnification; (b, c) SEM images of the end of the V_3O_7 nanowire and the end of GSs in VGS, respectively; (d) TEM images of VGS (the inset gives an HRTEM image of a V_3O_7 nanowire in GSs); (e) TEM image of the edge of VGS, showing a multilayer graphene coating; (f) SEM image and corresponding EDS line scan of VGS, showing the scanning route (green line), the element distribution of vanadium (red line), and carbon (yellow line), respectively.

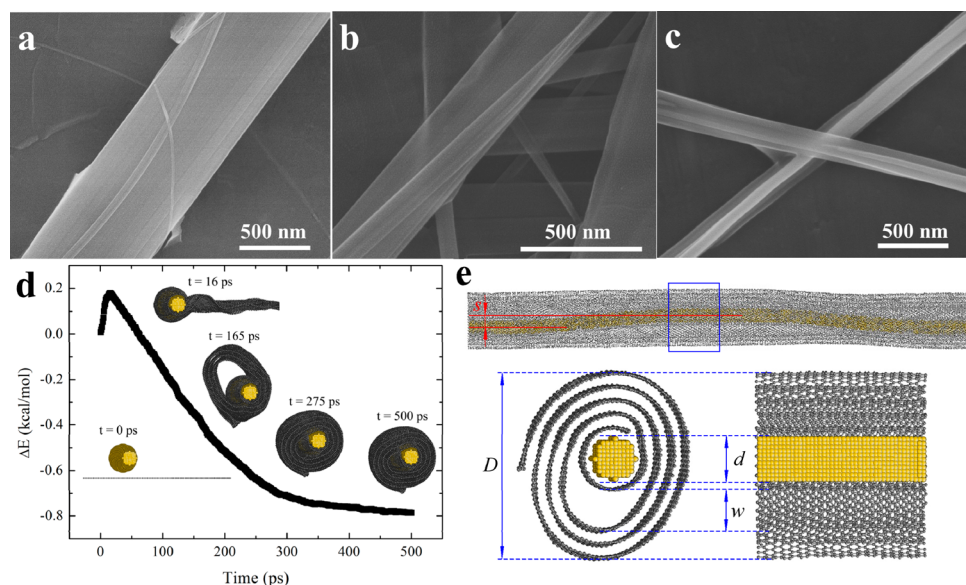


Figure 3. Formation mechanisms of VGS: (a–c) SEM images of VGS with hydrothermal reaction times of (a) 12 h, (b) 24 h, and (c) 48 h; (d) change in per-carbon energy during the wrapping of a graphene sheet onto a nanowire to form a GS (the insets are a series of simulation configurations of the formed GSs); (e) full view, partial enlarged view, and cross-section view of the MD snapshot of the nanowire templated graphene scroll semihollow structure.

than that of VGS with hollow channels. The lattice spacings of 0.483 and 0.468 nm match well with the separations between (130) and (200) planes, respectively. The V_3O_7 nanowires show a preferred {130} growth orientation. Transferring to the edge of VGS (Figure 2e), the specific lattice fringe of 7–10 layers of graphene can be observed with a lattice spacing of 0.734 nm. Furthermore, we can find an overlap between rGO sheets. According to the circumference formula, this indicates that at least two pieces of graphene sheets had rolled around

the V_3O_7 nanowire in each segment of the VGS (details are described in the Supporting Information). An EDS line scan (Figure 2f) further confirms that the V_3O_7 nanowires are in the GS cavity with obvious semihollow tubes.

The construction and formation mechanisms of the VGS have been investigated through a joint experimental–MD simulation. The growth mechanisms of oriented assembly and self-scroll are proposed to demonstrate the complicated architecture processes. The oriented assembly mechanism

describes the spontaneous self-organization of adjacent materials, so that they can react with each other, followed by the joining of these materials at a planar interface. In the reaction, V_3O_7 nanowires form for the strong orientation growth of $\{130\}$ in a short time (less than 12 h in this case). Then, the oriented assembly can guide the graphene sheets to assemble on the V_3O_7 nanowire surface and self-assemble to a graphene nanoribbon (Figure 3a). Later, the graphene nanoribbon tends to scroll surrounding the V_3O_7 nanowires, leading to a decrease in the graphene ribbons' width. The diameter of the graphene ribbon/scroll is calculated through statistics and decreases from over 200 nm (Figure 3b, c) to less than 150 nm (Figure S3, Supporting Information) with an increase of reaction time. The self-scroll process can be deduced through the decrease of graphene scroll diameter with increasing reaction time. Further information about VGS is obtained by taking the SEM image along one VGS (Figure S4, Supporting Information). We find that two V_3O_7 nanowires are rolled in a GS with semihollow channels in it. The diameter of VGS is reduced by half, accompanied by the disappearance of one V_3O_7 nanowire in the cavity of the VGS. Meanwhile, the relative position of the two V_3O_7 nanowires is ever-changing in the GSs. It is demonstrated that the diameter of the VGS and the hollows in GSs are related to the space structure and the diameter of V_3O_7 nanowires.

Generally, rGO sheets dispersed in solution exhibit a trend toward agglomeration. However, the above experimental observation indicated that a graphene ribbon formed along the nanowire before it scrolled and wrapped the nanowire (Figure 3a). This argument is supported by further MD simulations using the reactive force field (ReaxFF) potential.^{44,45} The results indicate the formation of covalent bonds between the rGO sheet and vanadium oxides, which anchored the graphene sheets to the V_3O_7 nanowire and facilitated the formation of the graphene ribbon (Figure S5, Supporting Information). Details of the simulations are described in the Supporting Information. MD simulations have also been performed to investigate the wrapping process of a nanowire by a monolayer graphene ribbon (Supporting Information, movie 1). Formation of the VGS involves competition among the bending energy of the graphene ribbon, the graphene–nanowire interaction energy, and the graphene–graphene interlayer interaction energy.^{23,46,47} The graphene sheet starts to wrap the nanowire due to the graphene–nanowire interaction energy, which increases the bending energy of the graphene ribbon. After the first layer of the GS was formed, the wrapping process proceeded spontaneously, since the lower energy states indicate that the GSs are more stable (Figure 3d). During the simulations, the system was equilibrated at $T = 450$ K, which is consistent with experiment. As far as we know, the interior cavity in the nanowire templated graphene scroll nanoarchitecture has never been reported in previous studies.^{22,23,28,45} According to the experimental observation, the V_3O_7 nanowires are wrapped in GSs with some curves, as shown in Figure S4 (Supporting Information). To clarify how the observed nanowire templated graphene scroll nanostructure with a semihollow cavity is formed, various simulations are carried out with straight nanowires as well as curved nanowires which are preset to have a certain bending structure. We find that when the graphene ribbon scrolls and wraps a nonstraight nanowire, an interior cavity is formed (Figure 3e). However, the hollow structure cannot be found in the simulations of the nonstraight nanowire wrapped by a single graphene sheet or of

the straight nanowires wrapped by a graphene ribbon (Figure S6, Supporting Information).

On the basis of the experimental data and simulation results, we propose the mechanism of the oriented assembly and self-scroll processes as follows. First, the competing growth reaction of V_3O_7 between the homogeneous nucleation in solution and heterogeneous nucleation on graphene sheets plays an important role. In this step, high vanadium sol concentration and rapid heating are needed to ensure that the homogeneous nucleation dominates the reaction process, which results in the rapid growth of V_3O_7 nanowires. Second, the bonding of the graphene and nanowire leads to a more steady energy state than the agglomeration of the graphene sheets does. Consequently, the graphene sheets are anchored on the surface of the nanowires and form a ribbon. When the graphene ribbon wraps a curved nanowire, the film tension inside the ribbon will promote the formation of GSs with hollow cavities rather than tight wraps of the GSs onto the nanowire. Third, the edge of the graphene ribbon starts to wrap the nanowire due to an attractive interaction between the graphene and nanowire. Fourth, the graphene ribbon bends along the surface of the nanowire and forms the GSs. Because of the curved nanowire structural template, the GSs cannot become tightly cocooned onto the nanowire. To reduce the bending energy along the nanowire, the GSs enlarge the diameter of the scroll core and form a semihollow structure. As shown in Figure 3e, D is the diameter of the VGS, which is the sum of the diameter of the nanowire d , the width of the semihollow channel w , and the thickness of the graphene multilayers h . MD results indicate that the width of this hollow channel w is determined by the bending deflection of nanowires s (Figure S7, Supporting Information): i.e., $w \approx s$. If $s \geq 2.5 d$, the nanowire cannot be fully wrapped by the graphene ribbon (Figure S8, Supporting Information). On the basis of experiments and calculations, h is a small value in comparison with D . Thus, we can propose a relationship to estimate the diameter of the VGS, $D = d + s$ (Supporting Information, part 2). Consequently, a different width of the semihollow can be achieved by controlling the size of graphene, the reaction time, and the curvature of nanowire.

The approaches above enabled us to fabricate lithium batteries with bicontinuous electron and lithium ion transfer channels in the electrode material, as shown in Figure 4a. During lithiation, electrolyte can enter the inner hollow space due to the capillarity effect^{48,49} and the lithium ion can react with the inner V_3O_7 nanowire directly. Meanwhile, the VGSs will bend and wrap with each other to relax the strain energy. During delithiation, the V_3O_7 nanowires shrink back. The VGS structure provides three attractive features as an electrode material in comparison to pure V_3O_7 nanowires: (1) the semihollow channels in the GSs provide space for free volume expansion of V_3O_7 nanowires and a continuous lithium ion transfer channel; (2) the GSs form a continuous electron transfer channel during charging and avoid the agglomeration of V_3O_7 nanowires; (3) the semihollow channel of GSs can limit the dissolution of V_3O_7 . At a current density of 2000 mA g⁻¹, the initial discharge capacities of VGS and VG (simply mixed with graphene; Figure S9b, Supporting Information) are 158 and 140 mAh/g, respectively. The discharge capacities change to 138 and 100 mAh/g after 400 cycles, corresponding to capacity retentions of 87.3% and 71.4% , respectively (Figure 4b). The PV, without mixing with graphene (Figure S9a, Supporting Information), shows a poor capacity that is lower than 50 mAh/g. The TEM images of VGS show that the

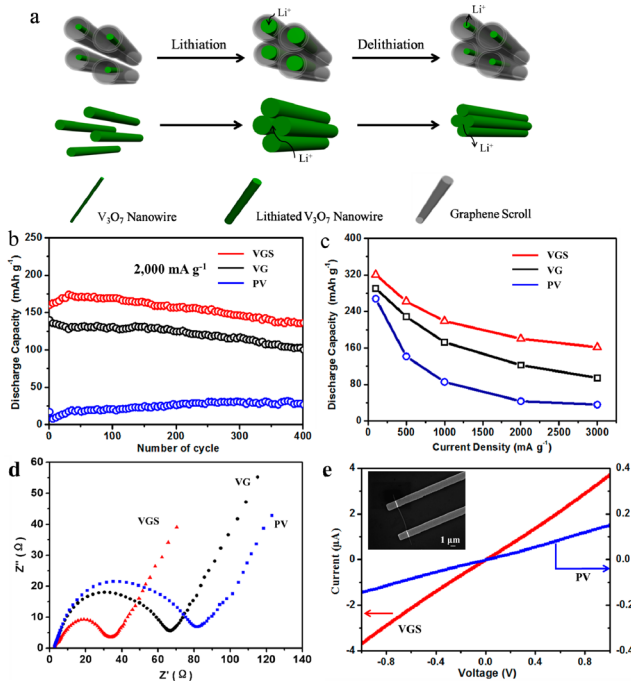


Figure 4. Electrochemical and electrical characterization of VGS. (a) Schematic of the VGS nanoarchitecture with continuous electron and Li ion transfer channels. The nanowire templated graphene scroll nanostructure provides internal void space for swelling during lithiation and an effective internal electrolyte channel to enhance the ion diffusion coefficient. In a pure nanowire structure, the strain could not be completely and promptly released. The nanowires tend to aggregate during cycles, leading to poor cycling performance. (b) Galvanostatic discharge profiles of VGS (red line), VG (black line), and PV (blue line) at 2000 mA/g tested between 4 and 1.5 V. (c) Galvanostatic discharge profiles of VGS, VG, and PV cycled at various currents from 100 to 3000 mAh/g tested between 4 and 1.5 V. (d) Impedance measurements for VGS, VG, and PV at the initial state. (e) Single-nanowire transport properties of VGS and PV (the inset is the SEM image of a VGS single-nanowire device).

structure of the VGS can be kept intact even after 400 times of cycling at 2 A/g (Figure S10, Supporting Information). The discharge capacities are measured in the voltage window from 1.5 to 4 V at current densities of 100, 500, 1000, 2000, and 3000 mA/g. VGS, VG, and PV all show high capacities of 321, 290, and 267.9 mAh/g at 100 mA/g (Figure S11, Supporting Information). At a very high current density of 3000 mA/g VGS still maintains a high capacity of 162 mAh/g, which is 1.7 and 4.5 times higher than those of VG and PV, respectively (Figure 4c). EIS is employed to understand why the VGS shows a better electrochemical performance (Figure 4d). The charge transfer resistances (R_{ct}) of VGS, VG, and PV are 32, 63, and 81 Ω, respectively. Further information is given by testing the I - V characteristics of a single nanowire (Figure 4e). With an effective length and cross section of the VGS at approximately 4.98 μm and 89.5²π nm², respectively, we calculate the conductivity value to be as high as 1056 S/m, which is 27 times higher than that of PV. This value can range from 800 to 1500 S/m depending on the different lengths and diameters of the samples. The above results demonstrated that (1) the electrochemical performance of V₂O₅ nanowires is enhanced with only 5 wt % graphene sheets added, (2) the graphene sheets scrolled on the surface of the nanowire are much more efficient than simply mixed sheets with nanowires

for enhancing the conductivity, (3) the VGS shows better cycling stability than VG due to the hollow channel and stable structure of the nanowire templated graphene scroll architecture.

To further identify the oriented assembly and self-scroll strategy, the MGS was constructed through the hydrothermal method. The crystal structures of MGS have been characterized by XRD measurements, which show that the MnO₂ nanowire and MGS are indexed to α -MnO₂ (072–1982) (Figure S12, Supporting Information). The SEM observations indicate that ultralong MGSs have been obtained (Figure 5a), which is

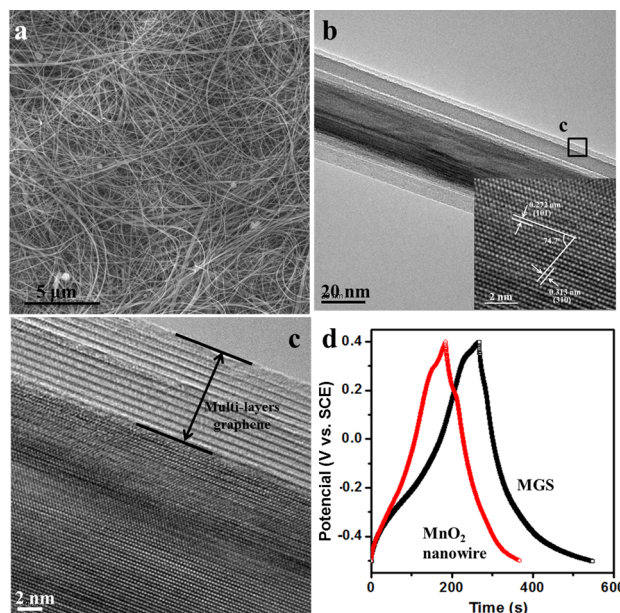


Figure 5. Structural and electrochemical characterization of MGS: (a) SEM image of synthesized MGS at low magnification; (b) TEM images of MGS (the inset is an HRTEM image of MnO₂ nanowire in GSS); (c) TEM image of the edge of MGS, showing multilayer graphene coating; (d) Galvanostatic charge/discharge curves measured at a constant current density of 1 A/g for MnO₂ nanowire and MGS in 2 M KOH.

consistent with the VGS results. The TEM images of the MGS (Figure 5b) demonstrate that the MnO₂ nanowires have been scrolled into the graphene scroll. The lattice spacings of 0.272 and 0.313 nm match well with the separations between (101) and (310) planes, respectively. At the edge of the MGS (Figure 5c) the graphene layer can be observed clearly. Then, the electrochemical performance of pure α -MnO₂ nanowires and MGSs were tested by fabricating a supercapacitor (Figure 5d). On the basis of the discharging curve line, the specific capacitance of the MGS is calculated to be 317 F/g at 1 A/g, which is over 1.5 times greater than that of the MnO₂ nanowire (194 F/g). It is demonstrated that the nanowire templated semihollow bicontinuous graphene scrolls can improve the performance of material in other systems as well.

CONCLUSION

Semihollow bicontinuous VGS and MGS over 30 μm in length have been obtained. The construction processes and the relationship among the width of the semihollow, the curvature of the nanowire, the size of graphene, and the reaction time are defined and explained by combining experiments and MD simulations. The unique structure of VGS provides space for

the volume expansion and shows the space confining effect for inhibiting the agglomeration of V_3O_7 nanowire, thus leading to remarkable electrochemical properties. Lithium ion battery cathodes made of VGS exhibit a high reversible capacity of 321 mAh/g at 100 mA/g and 87.3% capacity retention after 400 cycles at 2000 mA/g. Even at a high current density of 3000 mA/g, a reversible capacity of 162 mAh/g can be achieved with only 5 wt % graphene added, which is 4.5 times as high as that of pure V_3O_7 nanowires. The supercapacitor made of MGS also shows a high capacity of 317 F/g at 1 A/g, which is over 1.5 times greater than that of the MnO_2 nanowire. These results demonstrates that constructing VGS by combining oriented assembly and self-scroll is a significant and facile route to improve electrochemical properties with low quantities of graphene. The nanowire templated graphene scroll nano-architecture described in this paper will be a unique structure that has potential applications in energy storage and other fields.

ASSOCIATED CONTENT

Supporting Information

Text, figures, and an AVI file giving procedures and additional data. This material is available free of charge via the Internet at <http://pubs.acs.org>.

AUTHOR INFORMATION

Corresponding Author

*mlq518@whut.edu.cn; wuha@ustc.edu.cn; hch5927@whut.edu.cn.

Author Contributions

[†]These authors contributed equally.

Notes

The authors declare no competing financial interest.

ACKNOWLEDGMENTS

This work was supported by the National Basic Research Program of China (2013CB934103, 2012CB933003), the National Natural Science Foundation of China (51302203, 51272197 and 11172289), the International Science & Technology Cooperation Program of China (2013DFAS0840), the Program for New Century Excellent Talents in University (NCET-10-0661), and the Fundamental Research Funds for the Central Universities (2012-II-001, 2012-YB-02). Thanks are due to Professor C. M. Lieber of Harvard University and Professor Q. J. Zhang of Wuhan University of Technology for strong support and stimulating discussions. Special thanks are given to J. Liu of Pacific Northwest National Laboratory for his careful supervision, strong support, and stimulating discussions.

REFERENCES

- (1) Lee, C.; Wei, X.; Kysar, J. W.; Hone, J. *Science* **2008**, *321*, 385.
- (2) Liu, F.; Ming, P.; Li, J. *Phys. Rev. B* **2007**, *76*, 064120.
- (3) Bae, S.; Kim, H.; Lee, Y.; Xu, X.; Park, J.-S.; Zheng, Y.; Balakrishnan, J.; Lei, T.; Kim, H. R.; Song, Y. I. *Nat. Nanotechnol.* **2010**, *5*, 574.
- (4) Mayorov, A. S.; Gorbachev, R. V.; Morozov, S. V.; Britnell, L.; Jalil, R.; Ponomarenko, L. A.; Blake, P.; Novoselov, K. S.; Watanabe, K.; Taniguchi, T. *Nano Lett.* **2011**, *11*, 2396.
- (5) Morozov, S.; Novoselov, K.; Katsnelson, M.; Schedin, F.; Elias, D.; Jaszczak, J.; Geim, A. *Phys. Rev. Lett.* **2008**, *100*, 016602.
- (6) Balandin, A. A. *Nat. Mater.* **2011**, *10*, 569.
- (7) Zhu, Y.; Murali, S.; Stoller, M. D.; Ganesh, K.; Cai, W.; Ferreira, P. J.; Pirkle, A.; Wallace, R. M.; Cychoz, K. A.; Thommes, M. *Science* **2011**, *332*, 1537.
- (8) Wang, H.; Cui, L.-F.; Yang, Y.; Sanchez Casalongue, H.; Robinson, J. T.; Liang, Y.; Cui, Y.; Dai, H. *J. Am. Chem. Soc.* **2010**, *132*, 13978.
- (9) Yu, G.; Hu, L.; Vosgueritchian, M.; Wang, H.; Xie, X.; McDonough, J. R.; Cui, X.; Cui, Y.; Bao, Z. *Nano Lett.* **2011**, *11*, 2905.
- (10) Zhou, X.; Wang, F.; Zhu, Y.; Liu, Z. *J. Mater. Chem.* **2011**, *21*, 3353.
- (11) Li, Y.; Wang, H.; Xie, L.; Liang, Y.; Hong, G.; Dai, H. *J. Am. Chem. Soc.* **2011**, *133*, 7296.
- (12) Yang, S.; Feng, X.; Ivanovici, S.; Müllen, K. *Angew. Chem., Int. Ed.* **2010**, *49*, 8408.
- (13) Lu, Y.; Goldsmith, B. R.; Kybert, N. J.; Johnson, A. C. *Appl. Phys. Lett.* **2010**, *97*, 083107.
- (14) Liang, Y.; Li, Y.; Wang, H.; Zhou, J.; Wang, J.; Regier, T.; Dai, H. *Nat. Mater.* **2011**, *10*, 780.
- (15) Scheuermann, G. M.; Rumi, L.; Steurer, P.; Bannwarth, W.; Mühlaupt, R. *J. Am. Chem. Soc.* **2009**, *131*, 8262.
- (16) Kuila, T.; Bose, S.; Khanra, P.; Mishra, A. K.; Kim, N. H.; Lee, J. H. *Biosens. Bioelectron.* **2011**, *26*, 4637.
- (17) Liu, X.; Wang, F.; Aizen, R.; Yehezkel, O.; Willner, I. *J. Am. Chem. Soc.* **2013**, *135*, 11832.
- (18) Zhong, Z.; Wang, D.; Cui, Y.; Bockrath, M. W.; Lieber, C. M. *Science* **2003**, *302*, 1377.
- (19) Yan, R.; Gargas, D.; Yang, P. *Nat. Photonics* **2009**, *3*, 569.
- (20) Rao, A.; Richter, E.; Bandow, S.; Chase, B.; Eklund, P.; Williams, K.; Fang, S.; Subbaswamy, K.; Menon, M.; Thess, A. *Science* **1997**, *275*, 187.
- (21) Patra, N.; Wang, B.; Král, P. *Nano Lett.* **2009**, *9*, 3766.
- (22) Zhang, Z.; Li, T. *Appl. Phys. Lett.* **2010**, *97*, 081909.
- (23) Shi, X.; Cheng, Y.; Pugno, N. M.; Gao, H. *Appl. Phys. Lett.* **2010**, *96*, 053115.
- (24) Shi, X.; Cheng, Y.; Pugno, N. M.; Gao, H. *Small* **2010**, *6*, 739.
- (25) Zeng, F.; Kuang, Y.; Liu, G.; Liu, R.; Huang, Z.; Fu, C.; Zhou, H. *Nanoscale* **2012**, *4*, 3997.
- (26) Deng, J.; Ji, H.; Yan, C.; Zhang, J.; Si, W.; Baunack, S.; Oswald, S.; Mei, Y.; Schmidt, O. G. *Angew. Chem., Int. Ed.* **2013**, *125*, 2382.
- (27) Mai, L.; Wei, Q.; An, Q.; Tian, X.; Zhao, Y.; Xu, X.; Xu, L.; Chang, L.; Zhang, Q. *Adv. Mater.* **2013**, *25*, 2968.
- (28) Patra, N.; Song, Y.; Král, P. *ACS Nano* **2011**, *5*, 1798.
- (29) Li, Y.; Li, H.; Zhang, K.; Liew, K. M. *Carbon* **2012**, *50*, 566.
- (30) Yan, K.; Xue, Q.; Xia, D.; Chen, H.; Xie, J.; Dong, M. *ACS Nano* **2009**, *3*, 2235.
- (31) Volicis, L. M.; Mack, J. J.; Kaner, R. B. *Science* **2003**, *299*, 1361.
- (32) Iijima, S. *Nature* **1991**, *354*, 56.
- (33) Xie, X.; Ju, L.; Feng, X.; Sun, Y.; Zhou, R.; Liu, K.; Fan, S.; Li, Q.; Jiang, K. *Nano Lett.* **2009**, *9*, 2565.
- (34) Li, H.; Wu, J.; Qi, X.; He, Q.; Liusman, C.; Lu, G.; Zhou, X.; Zhang, H. *Small* **2013**, *9*, 382.
- (35) Zeng, F.; Kuang, Y.; Wang, Y.; Huang, Z.; Fu, C.; Zhou, H. *Adv. Mater.* **2011**, *23*, 4929.
- (36) Mpourmpakis, G.; Tylianakis, E.; Froudakis, G. E. *Nano Lett.* **2007**, *7*, 1893.
- (37) Jiang, K.; Li, Q.; Fan, S. *Nature* **2002**, *419*, 801.
- (38) Zheng, L.; O'Connell, M.; Doorn, S.; Liao, X.; Zhao, Y.; Akhadov, E.; Hoffbauer, M.; Roop, B.; Jia, Q.; Dye, R. *Nat. Mater.* **2004**, *3*, 673.
- (39) Schaper, A. K.; Hou, H.; Wang, M.; Bando, Y.; Golberg, D. *Carbon* **2011**, *49*, 1821.
- (40) Hummers, W. S., Jr.; Offeman, R. E. *J. Am. Chem. Soc.* **1958**, *80*, 1339.
- (41) Liang, Y.; Li, Y.; Wang, H.; Zhou, J.; Wang, J.; Regier, T.; Dai, H. *Nat. Mater.* **2011**, *10*, 780.
- (42) Plimpton, S. *J. Comput. Phys.* **1995**, *117*, 1.
- (43) Stuart, S. J.; Tutein, A. B.; Harrison, J. A. *J. Chem. Phys.* **2000**, *112*, 6472.

- (44) Chenoweth, K.; Duin, A. C.; Persson, P.; Cheng, M.-J.; Oxgaard, J.; Goddard, I.; William, A. *J. Phys. Chem. C* **2008**, *112*, 14645.
- (45) Chenoweth, K.; van Duin, A. C.; Goddard, W. A. *J. Phys. Chem. A* **2008**, *112*, 1040.
- (46) Braga, S. F.; Coluci, V. R.; Legoaas, S. B.; Giro, R.; Galvão, D. S.; Baughman, R. H. *Nano Lett.* **2004**, *4*, 881.
- (47) Wang, T.; Zhang, C.; Chen, S. *J. Nanosci. Nanotechnol.* **2013**, *13*, 1136.
- (48) Py, C.; Reverdy, P.; Doppler, L.; Bico, J.; Roman, B.; Baroud, C. *N. Phys. Rev. Lett.* **2007**, *98*, 156103.
- (49) Zhao, Y.; Xu, L.; Mai, L.; Han, C.; An, Q.; Xu, X.; Liu, X.; Zhang, Q. *Proc. Natl. Acad. Sci. U.S.A.* **2012**, *109*, 19569.